Journal of General Virology (2011), **92**, 1127–1140 DOI 10.1099/vir.0.028936-0

Severe acute respiratory syndrome coronavirus papain-like protease suppressed alpha interferon-induced responses through downregulation of extracellular signal-regulated kinase 1-mediated signalling pathways

Shih-Wein Li,[1,2] Chien-Chen Lai,[2,3] Jia-Fong Ping,[1] Fuu-Jen Tsai,[3] Lei Wan,[3] Ying-Ju Lin,[3] Szu-Hao Kung[4] and Cheng-Wen Lin[1,5,6]

Correspondence
Cheng-Wen Lin
cwlin@mail.cmu.edu.tw
Chien-Chen Lai
lailai@dragon.nchu.edu.tw

[1]Department of Medical Laboratory Science and Biotechnology, China Medical University, Taichung, Taiwan, ROC

[2]Institute of Molecular Biology, National Chung Hsing University, Taichung, Taiwan, ROC

[3]Department of Medical Genetics and Medical Research, China Medical University Hospital, Taichung, Taiwan, ROC

[4]Department of Biotechnology and Laboratory Science in Medicine, National Yang Ming University, Taipei, Taiwan, ROC

[5]Clinical Virology Laboratory, Department of Laboratory Medicine, China Medical University Hospital, Taichung, Taiwan, ROC

[6]Department of Biotechnology, Asia University, Wufeng, Taichung, Taiwan, ROC

Severe acute respiratory syndrome coronavirus (SARS-CoV) papain-like protease (PLpro), a deubiquitinating enzyme, reportedly blocks poly I:C-induced activation of interferon regulatory factor 3 and nuclear factor kappa B, reducing interferon (IFN) induction. This study investigated type I IFN antagonist mechanism of PLpro in human promonocytes. PLpro antagonized IFN-α-induced responses such as interferon-stimulated response element- and AP-1-driven promoter activation, protein kinase R, 2′-5′-oligoadenylate synthetase (OAS), interleukin (IL)-6 and IL-8 expression, and signal transducers and activators of transcription (STAT) 1 (Tyr701), STAT1 (Ser727) and c-Jun phosphorylation. A proteomics approach demonstrated downregulation of extracellular signal-regulated kinase (ERK) 1 and upregulation of ubiquitin-conjugating enzyme (UBC) E2-25k as inhibitory mechanism of PLpro on IFN-α-induced responses. IFN-α treatment significantly induced mRNA expression of UBC E2-25k, but not ERK1, causing time-dependent decrease of ERK1, but not ERK2, in PLpro-expressing cells. Poly-ubiquitination of ERK1 showed a relationship between ERK1 and ubiquitin proteasome signalling pathways associated with IFN antagonism by PLpro. Combination treatment of IFN-α and the proteasome inhibitor MG-132 showed a time-dependent restoration of ERK1 protein levels and significant increase of ERK1, STAT1 and c-Jun phosphorylation in PLpro-expressing cells. Importantly, PD098059 (an ERK1/2 inhibitor) treatment significantly reduced IFN-α-induced ERK1 and STAT1 phosphorylation, inhibiting IFN-α-induced expression of 2′-5′-OAS in vector control cells and PLpro-expressing cells. Overall results proved downregulation of ERK1 by ubiquitin proteasomes and suppression of interaction between ERK1 and STAT1 as type I IFN antagonist function of SARS-CoV PLpro.

Received 15 November 2010
Accepted 21 January 2011

INTRODUCTION

Severe acute respiratory syndrome (SARS)-associated coronavirus (SARS-CoV) is a novel pandemic virus causing highly contagious respiratory disease with approximately a 10 % mortality rate (Hsueh *et al.*, 2004; Lee *et al.*, 2003; Tsang *et al.*, 2003). Pathology entails bronchial epithelial denudation, loss of cilia, multinucleated syncytial cells, squamous metaplasia and transendothelial migration of monocytes/macrophages and neutrophils into lung tissue (Hsueh *et al.*, 2004; Nicholls *et al.*, 2003). Haematological examination reveals lymphopenia, thrombocytopenia and

Supplementary figures are available with the online version of this paper.

leukopenia (Wang *et al.*, 2004b; Yan *et al.*, 2004) accompanied by rapid elevation in serum of inflammatory cytokines like gamma interferon (IFN-γ), interleukin (IL)-18, transforming growth factor beta, IL-6, IFN-gamma-inducible protein-10, monocyte chemoattractant protein-1 (MCP-1), monokine induced by IFN-gamma and IL-8, which stimulate recruitment of neutrophils, monocytes, and immune responder cells like natural killer (NK), T- and B-cells into the lungs and other organs (He *et al.*, 2006; Huang *et al.*, 2005; Wong *et al.*, 2004).

SARS-CoV genome is a 30 kb positive-stranded RNA with a 5′ cap and a 3′ poly(A) tract that contains 14 ORFs (Marra *et al.*, 2003; Rota *et al.*, 2003; Ziebuhr, 2004). The 5′ proximal and largest of these ORFs encodes two large overlapping replicase polyproteins 1a and 1ab (~ 450 and ~750 kDa, respectively) processed to produce non-structural proteins (nsps) primarily involved in RNA replication. Two specific embedded proteases, papain-like (PLpro) and 3C-like (3CLpro), mediate processing of 1a and 1ab precursors into 16 nsps (termed nsp1–16).

PLpro, located within nsp3, cleaves at nsp1/2, nsp2/3 and nsp3/4 boundaries using consensus motif LXGG (Barretto *et al.*, 2005; Lindner *et al.*, 2005; Thiel *et al.*, 2003), along with consensus cleavage sequence of cellular deubiquitinating enzymes. Modelling and crystal structures reveal correlation between SARS-CoV PLpro and the herpes virus-associated ubiquitin-specific protease, indicating potential deubiquitinating activity (Ratia *et al.*, 2006; Sulea *et al.*, 2005) observed in *in vitro* cleavage assays (Barretto *et al.*, 2005; Lindner *et al.*, 2005). Interestingly, one such *in vitro* deubiquitination assay measured the cleavage of ubiquitin-like protein, interferon (IFN)-induced 15 kDa protein (ISG15), from an ISG15-fusion protein, suggesting de-ISGylation by PLpro as a mechanism by which SARS-CoV inactivates IFN-α/β-induced innate immune response.

SARS-CoV infection does not induce type I IFNs in cell culture (Spiegel *et al.*, 2005). Recent reports reveal PLpro inhibiting the phosphorylation of interferon regulatory factor 3 (IRF-3) and type I IFN synthesis (Devaraj *et al.*, 2007) and antagonizing both IRF-3 and nuclear factor kappa B (NF-κB) signalling pathways (Frieman *et al.*, 2009). Still, the mechanisms of type I IFN antagonism by which SARS-CoV PLpro does this remain unclear. Type I interferons (IFNs, IFN-α, IFN-β and IFN-ω) mediate a wide range of biological activities: antiviral activity, immune response, differentiation, cell growth and apoptosis (Biron, 2001). IFN-α/β binds to a common heterodimeric receptor composed of IFN-α/β receptor 1 (IFNAR1) and IFN-α/β receptor 2 (IFNAR2), then activates Janus kinase (JAK) family plus signal transducers and activators of transcription (STATs) family (Tang *et al.*, 2007). Phosphorylation of STAT1 at tyrosine 701 by JAK1 is required for STAT1–STAT2 heterodimer formation and nuclear translocation (Banninger & Reich, 2004). Phosphorylation of STAT1 at serine 727 by extracellular signal-regulated kinase (ERK)1/2 and p38 mitogen-activated protein kinase (MAPK) facilitates interaction of STAT1 with basal transcription machinery for full expression of antiviral genes like protein kinase R (PKR), 2′-5′-oligoadenylate synthetase (OAS) and IFN-stimulated gene 15 (ISG15) (Deb *et al.*, 2003; Uddin *et al.*, 2002). Currently, IFN-α is also a widely used cytokine for treating human solid and haematologic malignancies (Tagliaferri *et al.*, 2005). IFN-α-mediated anti-tumour effect correlates with activation of JAK–STAT signalling pathway, resulting in upregulation of Fas/FasL and Jnk1/p38 stimulation signalling pathways. Escape mechanisms of IFN-α-mediated anti-tumour effect are likewise reported, e.g. EGF-mediated Ras/Raf/ERK1/2-dependent pathway, Akt- and NF-κB-dependent pathways and STAT3/PI3K-mediated signalling (Tagliaferri *et al.*, 2005). Some key regulators of signal transduction, e.g. JAK1, STAT1, ERK1 are demonstrably modified by ubiquitin conjugation (Malakhov *et al.*, 2003; Lu & Hunter, 2009), with over 100 ubiquitin-conjugated proteins encompassing diverse cellular pathways identified in antiviral innate immune responses (Giannakopoulos *et al.*, 2005; Zhao *et al.*, 2005), e.g. NF-κB-inducing kinase, critical regulator of non-canonical NF-κB pathway, is ubiquitinated and degraded by RING finger E3 ligases (Varfolomeev *et al.*, 2007). With SARS-CoV PLpro as a deubiquitinating enzyme, this points to specifically disrupting signal transduction of innate immune system against SARS-CoV infection.

Investigating possible effect of PLpro on the responses to type I IFNs is vital to the understanding of SARS pathogenesis. This study first demonstrated stable expression of SARS-CoV PLpro significantly inhibited IFN-α-induced responses like interferon-stimulated response element (ISRE)- and AP-1-driven promoter activation, gene expression of PKR, 2′-5′-OAS, IL-6 and IL-8, and phosphorylation of STAT1 and c-Jun. Downregulation of ERK1 was identified by comparative proteomic analysis of PLpro-expressing cells against control cells with respect to IFN-α response, correlating with potential antagonistic mechanism of SARS-CoV PLpro in response to IFN-α.

RESULTS

Expression of the SARS-CoV PLpro in human promonocytes

To characterize the effect of SARS-CoV PLpro on the intracellular innate immune response, human promonocyte HL-CZ (human promonocyte cell line) cells were co-transfected with the plasmid pSARS-CoV PLpro [expressing PLpro with herpes simplex virus (HSV) epitope tag] or empty control vector and GFP reporter plasmid followed by 2 weeks of treatment with G418 to select stably

transfected cells. Expression of PLpro was detected by immunofluorescent staining (Fig. 1a) and Western blotting (Fig. 1b), with vector-derived His-tag found in both empty vector- and pSARS-CoV PLpro-transfected cells and HSV-tag detected only in pSARS-CoV-PLpro-transfected cells. Western blotting of transfected cells' lysates with anti-HSV-tag antibodies revealed a 60 kDa band in pSARS-CoV-PLpro-transfected cells (Fig. 1b), but not in empty vector-transfected cells.

To determine if expressed PLpro was active, proteolytic activity in cell lysates was assayed by *in vitro trans*-cleavage, with HRP containing the LXGG motif recognized by PLpro as substrate. Fig. 1(c) shows significant reduction in HRP enzyme activity in the reaction containing lysates of PLpro-expressing cells, but not in the reaction with lysates from vector control cells. Lysates of PLpro-expressing cells also exhibited time-dependent *trans*-cleavage activity. SARS-CoV PLpro expressed in human promonocyte cells was thus enzymically active.

Inhibition of PLpro on IFN-α-induced ISRE- and AP-1-mediated activation

To test the effect of SARS-CoV PLpro on ISRE-mediated responses to IFN-α, activity of ISRE-driven reporter and

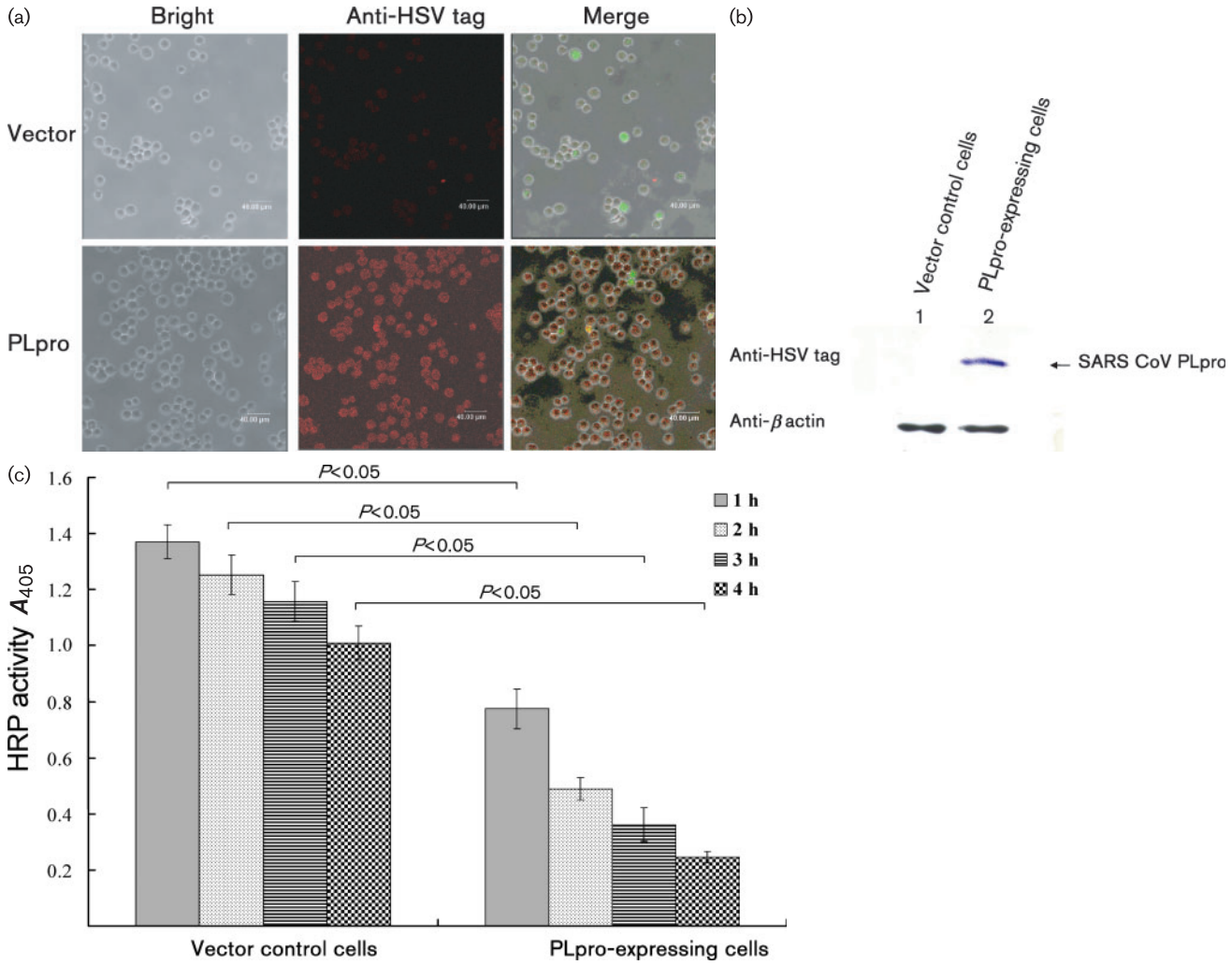

Fig. 1. Expression of SARS-CoV PLpro in human promonocyte HL-CZ cells. Cells transfected with pcDNA3.1 (control vector) plus pEGFP-N1 or pSARS-CoV-PLpro plus pEGFP-N1 were selected by a 2 week incubation with G418. The HSV-tag fusion protein was detected using immunofluorescence staining of anti-HSV tag antibody and rhodamine-conjugated anti-mouse IgG antibody (a). Lysates from cells transfected with pcDNA3.1 plus pEGFP-N1 (lane 1) or pSARS-CoV-PLpro plus pEGFP-N1 (lane 2) were analysed by 10% SDS-PAGE prior to blotting (b). The blot's upper half of was probed with anti-HSV antibody, the lower with anti-β actin antibody as internal control. *Trans*-cleavage activity of SARS-CoV PLpro in transfected cell lysates was further analysed (c). Following incubation of lysates from 10^6 PLpro-expressing cells and control vector cells with substrate HRP, residual HRP activity was measured as a mean of three independent experiments; error bars show SEM.

mRNA expression of ISRE-driven gene PKR in empty vector controls and PLpro-expressing cells were examined by dual luciferase reporter assay system (Fig. 2a) and quantitative real-time RT-PCR (Fig. 2b). Cells were co-transfected with *cis*-reporter plasmid containing firefly luciferase under the control of ISRE and an internal control reporter plasmid that constitutively expressed *Renilla* luciferase. After treatment with IFN-α for 4 h, expression of firefly luciferase was determined and normalized to *Renilla* luciferase expression. Fig. 2(a) plots vector control and PLpro-expressing cells' dose-dependent transcriptional activity of the ISRE promoter by IFN-α. ISRE promoter-driven luciferase activity in PLpro-expressing cells was half of that in vector control cells. The mRNA expression of specific ISRE-driven gene PKR was analysed in both types of cells in the absence or presence of IFN-α, using quantitative real-time RT-PCR assays (Fig. 2b). Induction of PKR by IFN-α was approximately sevenfold lower in PLpro-expressing cells than in control vector cells. Since the endogenous PKR promoter contains not only the ISRE element but also kinase-conserved sequence element for both basal and IFN-inducible PKR promoter activity (Samuel, 2001), the other specific ISRE promoter-driven gene 2′-5′-OAS was further analysed (Fig. 2c). Induction of 2′-5′-OAS by IFN-α was sixfold lower in PLpro-expressing cells than in vector controls. Results confirmed the antagonism of IFN-α-induced ISRE-mediated gene expression by PLpro.

Subsequently, the effect of SARS-CoV PLpro on AP-1-mediated responses to IFN-α was tested (Fig. 3). Activity of AP-1 enhancer in response to IFN-α was next determined by transient transfection with plasmid vector containing luciferase under the control of the AP-1 enhancer. Fig. 3(a) shows luciferase activity significantly induced in a dose-dependent manner in control vector cells by IFN-α, but induction using the

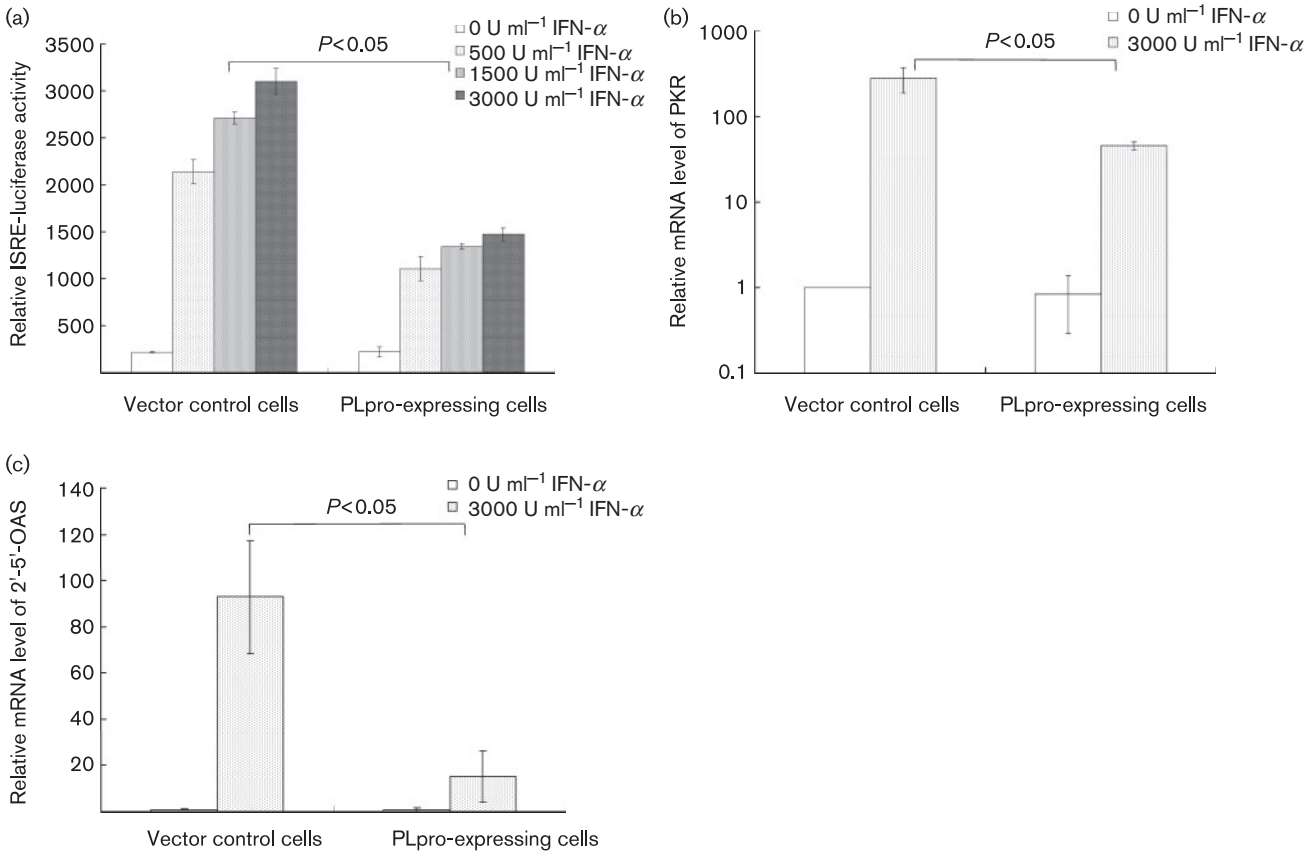

Fig. 2. Effect of PLpro on ISRE-mediated gene expression in response to IFN-α. (a) Vector control cells and PLpro-expressing cells were transiently co-transfected with reporter plasmid containing firefly luciferase under the control of the ISRE and an internal control reporter pRluc-C1 that constitutively expressed *Renilla* luciferase. After 4 h IFN-α treatment, firefly luciferase and *Renilla* luciferase were measured and firefly luciferase activity normalized to *Renilla* luciferase activity, as reported. Each bar is the mean of three independent experiments; error bar is SEM. The mRNA expressions of ISRE-driven gene PKR (b) and 2′-5′-OAS (c) in vector control cells and SARS PLpro-expressing cells untreated or treated was measured by quantitative real-time PCR. Relative fold levels of PKR or 2′-5′-OAS mRNA level appear as ratio of PKR or 2′-5′-OAS mRNA/GAPDH mRNA. Each bar graph is the mean of three independent experiments; error bars represent SEM.

same level of IFN-α totally absent in PLpro-expressing cells. These results indicate SARS-CoV PLpro-mediated suppression and AP-1-mediated promoter activity in response to IFN-α. Upon stimulation with IFN-α, a 15-fold increase in IL-6 mRNA was induced in vector control cells; no significant induction occurred in PLpro-expressing cells (Fig. 3b). Since the AP-1 element was also required for the IL-8 expression (Hoffmann *et al.*, 2002), thus IL-8 mRNA levels in response to IFN-α were also measured (Fig. 3c). Levels of IL-8 mRNA were 3.5-fold higher in both unstimulated and stimulated vector controls than in unstimulated and stimulated PLpro-expressing cells (Fig. 3c), suggesting interference by PLpro with basal level IL-8 mRNA transcription. AP-1 promoter activity and driven gene expression indicated SARS-CoV PLpro as significantly inhibiting mRNA expression of AP-1-mediated genes.

Downregulation of IFN-α-induced ERK1-mediated signalling by PLpro

For a global perspective mechanism of type I IFN antagonism by SARS-CoV PLpro, differential protein expression in vector control and PLpro-expressing cells in the absence or presence of IFN-α was analysed by two-dimensional (2D) gel electrophoresis and nanoscale capillary liquid chromatography/electrospray ionization Q-TOF MS to identify differentially regulated proteins. In Fig. 4(a), downregulated protein ERK1 and upregulated ubiquitin-conjugating enzyme (UBC) E2-25K appeared in 2D gels of IFN-α-treated PLpro-expressing cells, and then identified by trypsin digestion and NanoLC Trap Q-TOF MS analysis. ERK1 showed a Mascot score of 109, sequence coverage of 14 %, and two matched peptides; UBC E2-25K showed a Mascot score of 248, sequence coverage of 59 %, and four matched peptides. Peptide peaks from Q-TOF MS analysis from two representative spots of ERK1 and UBC

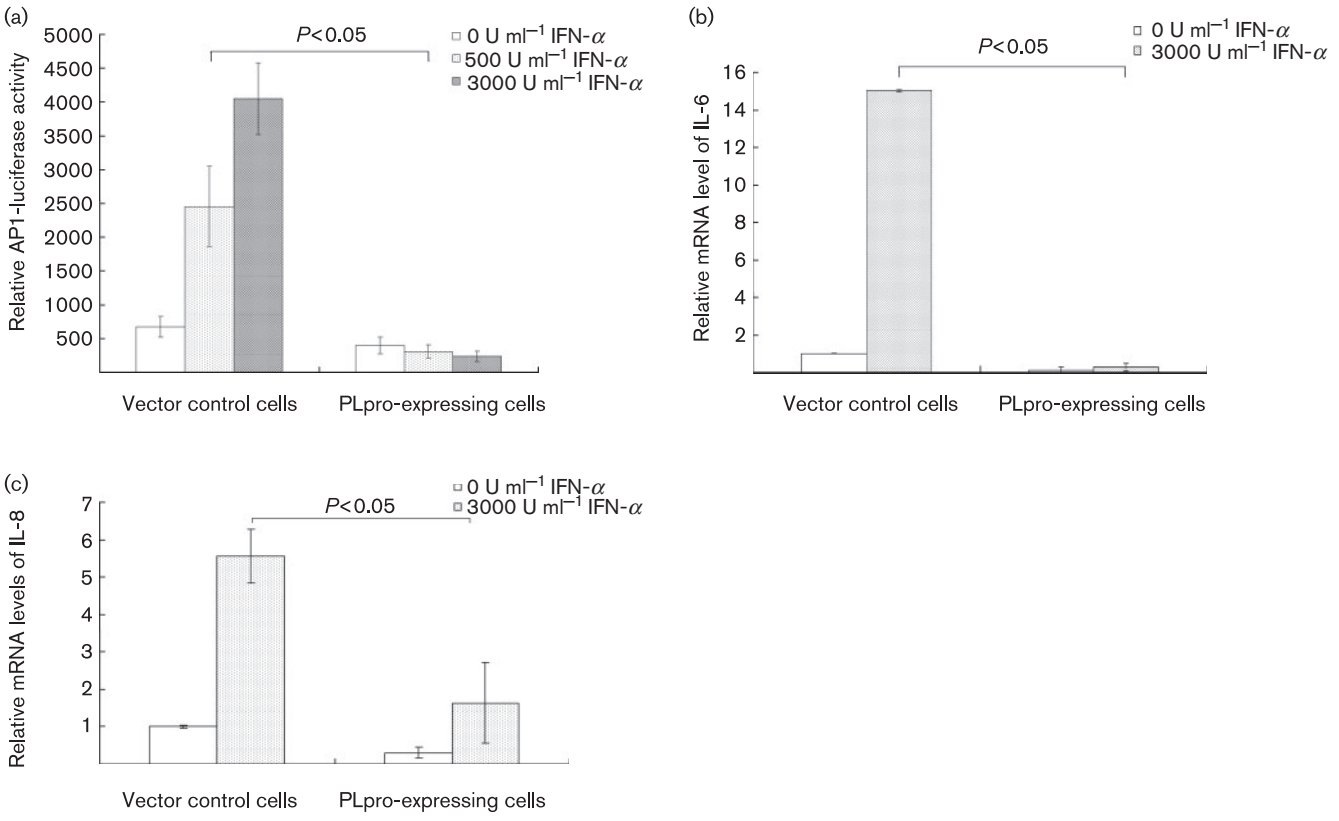

Fig. 3. Effect of PLpro on AP-1-mediated gene expression in response to IFN-α. (a) Vector control and PLpro-expressing cells were transiently co-transfected with reporter plasmid containing AP-1-driven firefly luciferase and an internal control reporter pRluc-C1 that constitutively expressed *Renilla* luciferase. After 4 h treatment with IFN-α, AP-1-driven firefly luciferase and *Renilla* luciferase were measured and firefly luciferase activity normalized to *Renilla* luciferase activity is reported. Each bar is the mean of three independent experiments; error bar is SEM. In addition, the mRNA expressions of AP-1-driven genes IL-6 (b) and IL-8 (c) in vector control cells and SARS PLpro-expressing cells untreated or treated was measured by quantitative real-time PCR. Relative fold levels of IL-6 or IL-8 mRNA level are presented as the ratio of IL-6 or IL-8 mRNA/GAPDH mRNA. Each bar on the graph is the mean of three independent experiments; error bars represent SEM.

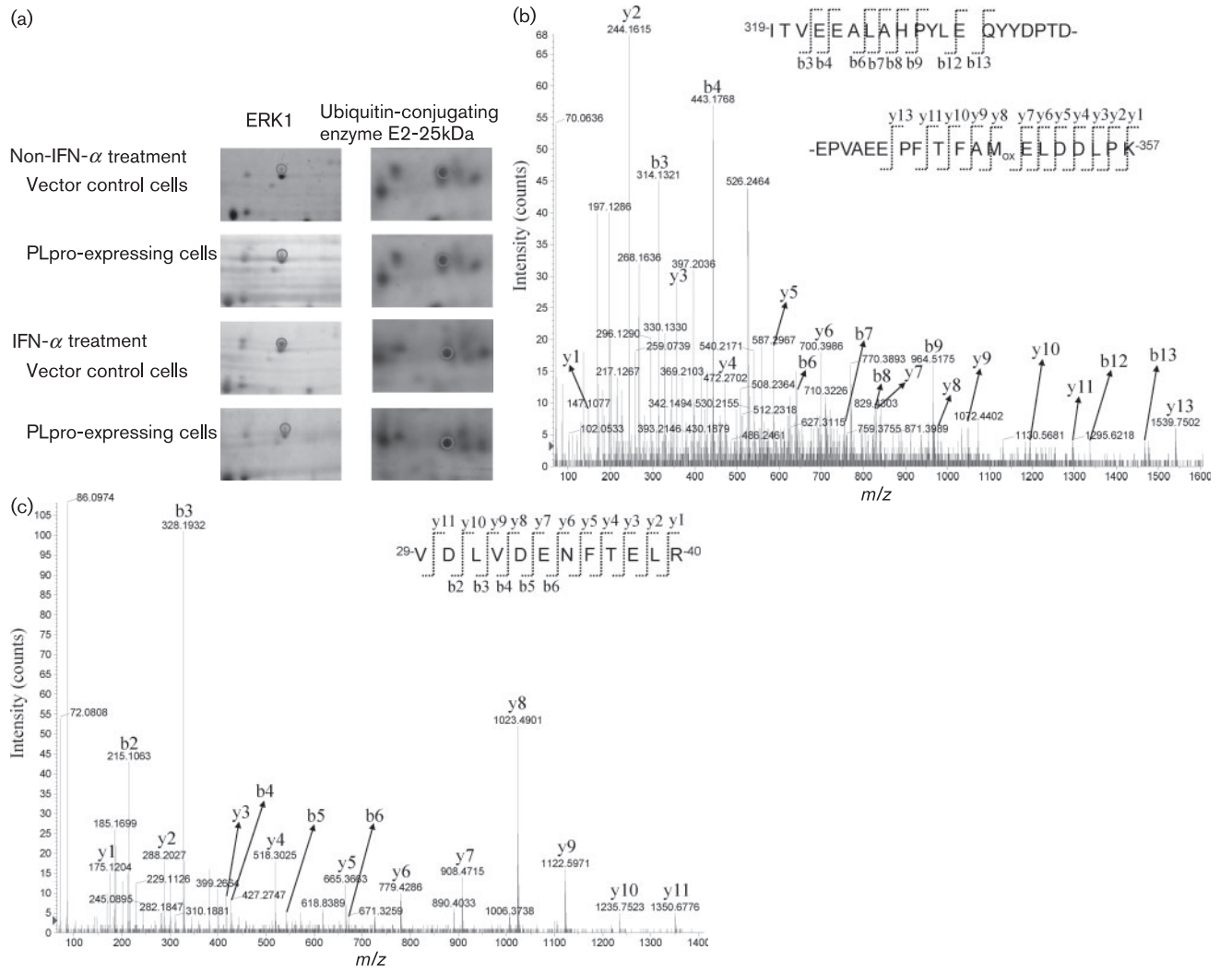

Fig. 4. Effect of SARS-CoV PLpro on protein profiles of vector control cells and PLpro-expressing cells in response to IFN-α. Total protein (100 μg) from control vector cells in the absence or presence of IFN-α or PLpro-expressing cells in the absence or presence of IFN-α was resolved by 2D electrophoresis. (a) Enlarged images of 2D gel electrophoresis of protein expression in PLpro-expressing cells and vector control cells in response to IFN-α treatment. (b) Nanoelectrospray mass spectrum of triply charged ion *m/z* 1514.77 for ERK1 is shown; ITVEEALAHPYLEQYYDPTDEPVAEEPFTFAM$_{ox}$ELDDLPK amino acid sequence was determined from mass differences in y- and b-fragment ions series and matched residues 319–357 of ERK1 (MAPK3). (c) Nanoelectrospray mass spectrum of the doubly charged ion *m/z* 725.41 for UBC E2-25k is shown. Amino acid sequence VDLVDENFTELR was determined from mass differences in y- and b-fragment ions series and matched residues 29–40 of ubiquitin-conjugating enzyme E2-25k. *Only y- and b-fragment ions are labelled in the spectrum.

E2-25K (Fig. 4b, c), respectively. ERK1 in particular is reported in several biological pathways (mitogen-activated protein kinase kinase, cytokine-mediated inflammation, IFN signalling pathways) and thus could play an important role in the mechanism of IFN-α antagonism by PLpro.

Upregulation of UBC E2-25K of ubiquitin proteasome pathways by PLpro

Quantitative RT-PCR was employed to determine expression levels of ERK1 and UBC E2-25K in PLpro-expressing and vector control cells in the absence or presence of IFN-α (Fig. 5). Amount of ERK1 mRNA showed no difference between vector control and PLpro-expressing cells, whether treated with IFN-α or not (Fig. 5a). Relative level of UBC E2-25K mRNA in PLpro-expressing cells was markedly higher than that in vector controls, with or without IFN-α treatment (Fig. 5b), proving that SARS-CoV PLpro activates the ubiquitin-proteasome system in human promonocyte cells. To compare ERK1 protein levels in vector control and PLpro-expressing cells in the presence or absence of IFN-α, ERK1 and ERK2 were measured by

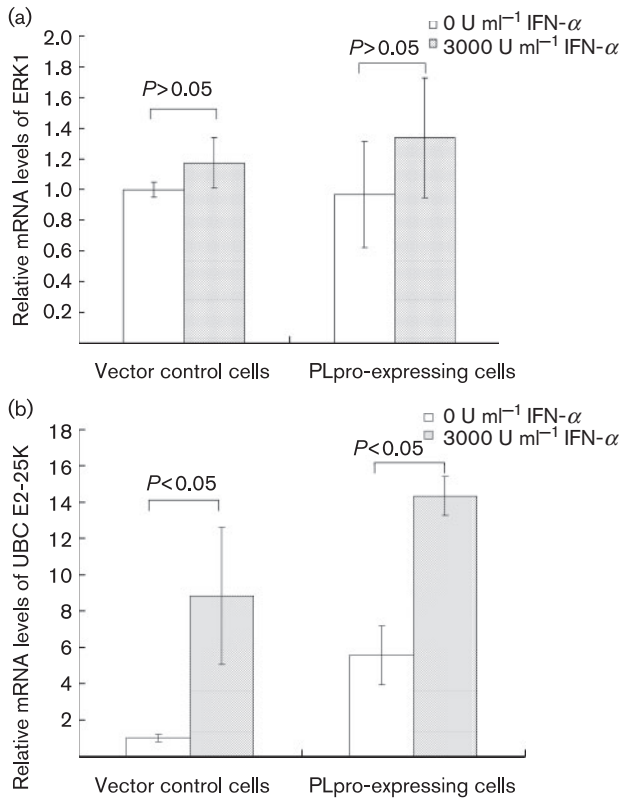

Fig. 5. Analysis of mRNA levels of ERK1 and UBC E2-25K in vector control cells and PLpro-expressing cells. Total RNA was extracted from vector control cells and PLpro-expressing cells treated with or without IFN-α (3000 U ml^{-1}) for 4 h and relative mRNA levels of ERK1 (a) and UBC E2-25K (b) were measured by quantitative real-time PCR. The relative fold levels of ERK1 and UBC E2-25K mRNA were presented as the ratio of indicated mRNA/GAPDH mRNA. Each bar on the graph is the mean of three independent experiments and the error bars represent the SEM.

Western blots with anti-p44/p42 (ERK1/2) mAb (Fig. 6a). Western blotting showed 42 kDa ERK2 protein levels roughly similar in vector control and PLpro-expressing cells, whereas the protein level of 44 kDa ERK1 in PLpro-expressing cells was near 50 % of that in controls (determined by densitometry normalized to β-actin protein control in each sample) (Fig. 6a, lanes 1–2). IFN-α treatment caused time-dependent reduction of ERK1, but not ERK2, in PLpro-expressing cells (Fig. 6a, lanes 4 and 6). Results confirmed data of 2D/MALDI TOF MS, which showed definite reduction of ERK1 in PLpro-expressing cells in response to IFN-α.

Since PLpro-expressing cells have no difference in mRNA amount, but a significant reduction of ERK1 protein levels by IFN-α, we suggest that upregulation of UBC E2-25k in PLpro-expressing cells could increase ubiquitination on ERK1, enhancing ERK1 degradation by IFN-α treatment. To test the hypothesis, ERK1 immunoprecipitation followed by Western blot probed with anti-ubiquitin antibodies was conducted in the absence or presence of IFN-α (Fig. 6b), revealing that ERK1 conjugated with different sizes of poly-ubiquitin chains, i.e. molecular sizes of 52, 60, 68, 76 and 84 kDa. Higher level of ERK1 ubiquitination was found in PLpro-expressing cells (Fig. 6b, lane 2) than in vector control cells (Fig. 6b, lane 1). Moreover, IFN-α treatment significantly reduced the level of ERK1 ubiquitination in PLpro-expressing cells (Fig. 6b, lane 4), not in vector controls (Fig. 6b, lane 3).

To test the correlation between upregulation of ubiquitin proteasome activity and downregulation of ERK1 in PLpro-expressing cells, the proteasome inhibitor MG-132 was added to analyse changes of ERK1 and ERK2 using Western blot assays with anti-p44/p42 (ERK1/2) mAb (Fig. 6c). Treatment with both IFN-α and the proteasome inhibitor MG-132 caused time-dependent increases of ERK1 and ERK2, in PLpro-expressing cells (Fig. 6c, lanes 2, 4, 6 and 8). The higher expression level of ERK2 than ERK1 was consistently observed in vector control and PLpro-expressing cells in responses to treatment with/without both IFN-α and the proteasome inhibitor MG-132. The increase of ERK1 level in PLpro-expressing cells correlated with treatment of the proteasome inhibitor MG-132, being not compensated by ERK2. After 1 h treatment with both IFN-α and MG-132, the overall amount of ERK1 in PLpro-expressing cells was equal to that in vector control cells (Fig. 6c, lanes 7 and 8). Results indicate that the proteasome inhibitor MG-132 blocked the escape of IFN-α-induced response by ERK1 degradation in PLpro-expressing cells, along with SARS-CoV PLpro enhancing ERK1 degradation by upregulating ubiquitin proteasome pathways in response to IFN-α, being associated with inhibiting IFN-α-induced ISRE- and AP-1 promoter activation and IFN-α-stimulated gene expression.

Inhibition of ubiquitin proteasome activity restored activation of IFN-α-induced ERK-mediated signalling in PLpro-expressing cells

To examine the effects of unbiquitin proteasome upregulation on ERK1-mediated signalling, the proteasome inhibitor MG-132 was added to analyse changes of the ERK1-mediated signalling pathway. Phosphorylation of ERK1, STAT1 and c-Jun in PLpro-expressing cells and vector control cells was subsequently analysed by Western blots with phosphorylation site-specific antibodies (Fig. 7). IFN-α treatment caused time-dependent ERK1 phosphorylation in vector controls (Fig. 7a, lanes 1, 3, 5 and 7), but only a transient period of ERK1 phosphorylation in PLpro-expressing cells (Fig. 7a, lane 4), probably due to lower ERK1 protein levels via degradation by ubiquitin-proteasome pathway in PLpro-expressing cells following IFN-α treatment (Fig. 6). Consistent with this hypothesis, treatment with both IFN-α and the proteasome inhibitor MG-132 restored IFN-α-induced activation of ERK1 in a time-dependent manner in PLpro-expressing cells (Fig. 7b, lanes 2, 4, 6 and 8). Treatment with IFN-α or both IFN-α

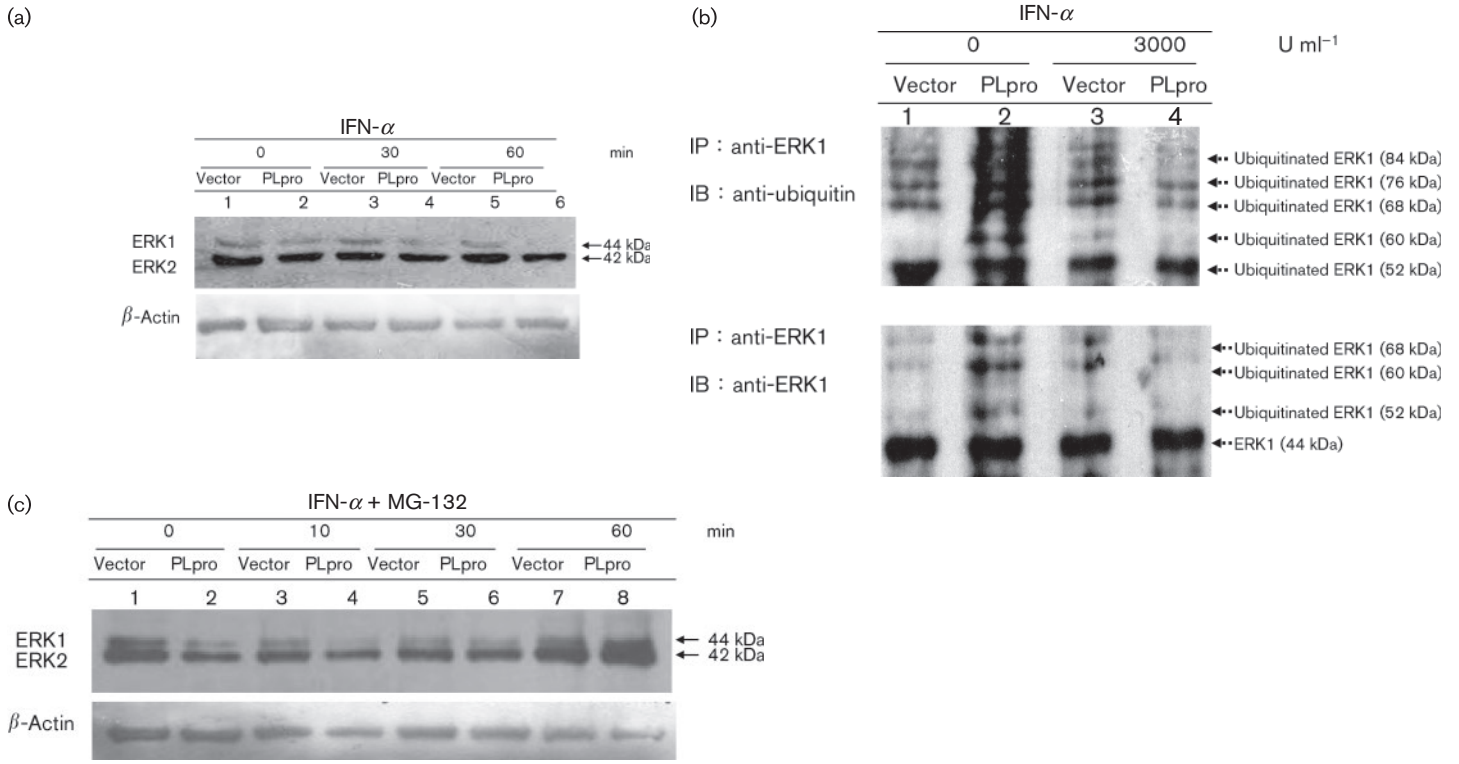

Fig. 6. Protein amount and ubiquitination level of ERK1 in vector control cells and PLpro-expressing cells. (a) Vector control cells and PLpro-expressing cells were treated with IFN-α (3000 U ml^{-1}) for 30 or 60 min. Cell lysates were Western blotted and probed with anti-ERK1/2 or anti-β-actin antibody as an internal control. (b) Vector control cells and PLpro-expressing cells were treated with or without IFN-α (3000 U ml^{-1}) for 60 min. Cell lysates were also immunoprecipitated with anti-ERK1 mAb, followed by Western blotting probed with either anti-ubiquitin or anti-ERK1 antibody. (c) Vector control cells and PLpro-expressing cells were treated with IFN-α and the proteosome inhibitor MG-132 (20 μM) for 10, 30 or 60 min. Cell lysates were Western blotted and probed with anti-ERK1/2 or anti-β-actin antibody as an internal control.

and the proteasome inhibitor MG-132 had no detectable band of phospho-ERK2 in vector control and PLpro-expressing cells. Subsequently, PLpro expression suppressed phosphorylation of STAT1 at Tyr701 and Ser727 sites in resting cells and in response to IFN-α treatment (Fig. 7a, lanes 4, 6 and 8). Treatment with the proteasome inhibitor MG-132 also significantly increased phosphorylation of STAT1 at Tyr701 and Ser727 sites in PLpro-expressing cells induced with IFN-α (Fig. 7b, lanes 4, 6 and 8). Moreover, phosphorylation of transcriptional factor c-Jun was assessed to find that the level of c-Jun phosphorylation was similar in both types of cells. Yet IFN-α treatment reduced c-Jun phosphorylation, meanwhile treatment with both IFN-α and MG-132 also significantly increased c-Jun phosphorylation in PLpro-expressing cells (Fig. 7a, b, lanes 4, 6 and 8). As expected, if PLpro-induced degradation of ERK1 suppresses STAT1 and c-Jun activation, inhibition of ubiquitin proteasome function with MG-132 heightened IFN-α-induced activation of ERK1-mediated signalling in PLpro-expressing cells.

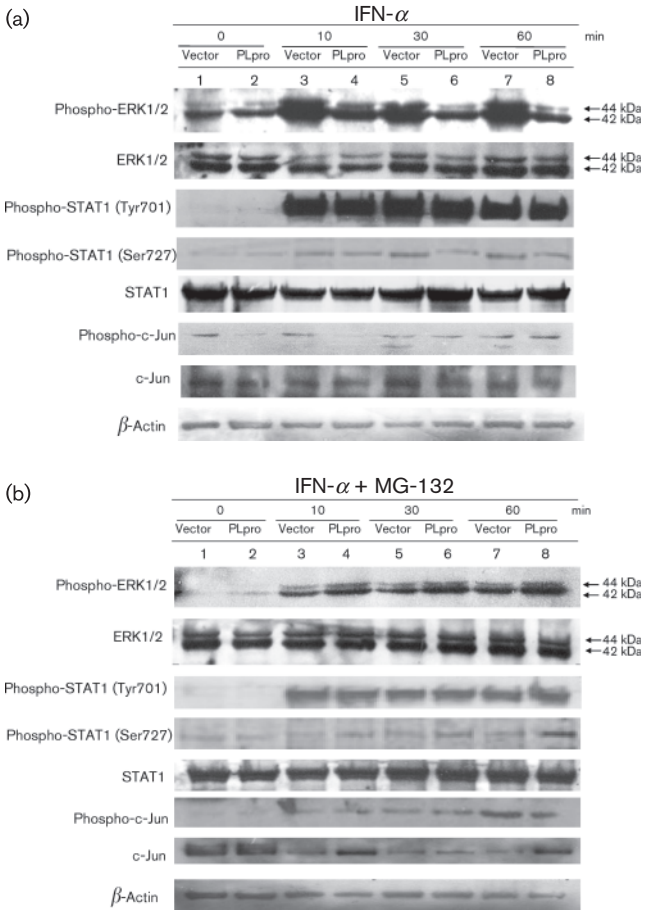

Fig. 7. Effect of the proteasome inhibitor MG-132 on IFN-α-induced phosphorylation of ERK1, STAT1 and c-Jun in vector control cells and PLpro-expressing cells. Vector control cells and PLpro-expressing cells were treated with IFN-α (3000 U ml^{-1}) (a) or IFN-α and the proteasome inhibitor MG-132 (20 μM) (b) for 10, 30 or 60 min. Cell lysates were subjected to Western blotting probed with anti-phospho-ERK1/2, anti-ERK1/2 anti-phospho-STAT1 (Tyr701), anti-phospho-STAT1 (Ser727), anti-STAT1, anti-phospho-c-Jun or anti-c-Jun antibodies. The relevant protein of the blot was probed with anti-β actin antibodies as an internal control.

Correlation of ERK1 phosphorylation with STAT1 signalling pathways

To confirm the effect of ERK1 phosphorylation on STAT1 signalling, inhibition of PD098059 (an ERK1/2 inhibitor) on ERK1 and STAT1 phosphorylation was analysed by Western blotting (Fig. 8). PD098059 treatment had inhibitory effects on IFN-α-induced ERK1 phosphorylation in vector control cells and PLpro-expressing cells (Fig. 8a, lanes 5–7; Fig. 8b, lanes 5–7). Importantly, PD098059 treatment also manifests inhibitory effects on STAT1 phosphorylation at Ser727, but not Tyr701 in vector control cells and PLpro-expressing cells in response to

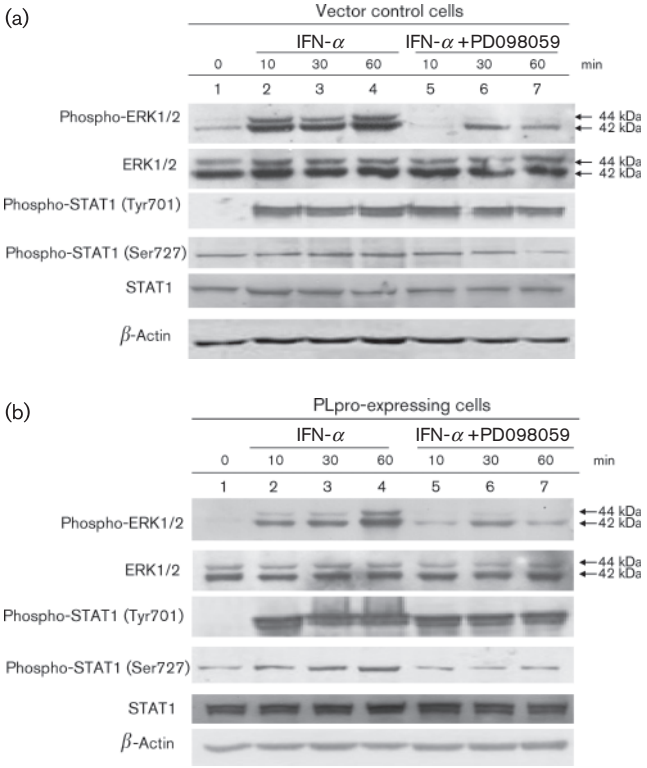

Fig. 8. Effect of PD098059 treatment on IFN-α-induced phosphorylation of ERK1 and STAT1 in vector control cells and PLpro-expressing cells. Vector control cells and PLpro-expressing cells were treated with IFN-α (a) or IFN-α and PD098059 (b) for 10, 30 or 60 min. Cell lysates were subjected to Western blotting probed with anti-phospho-ERK1/2, anti-ERK1/2, anti-phospho-STAT1 (Tyr701), anti-phospho-STAT1 (Ser727) or anti-STAT1 antibodies. The relevant protein of the blot was probed with anti-β actin antibodies as an internal control.

IFN-α treatment (Fig. 8a, lanes 5–7; Fig. 8b, lanes 5–7). In addition, effects of PD098059 treatment on IFN-α-induced ISRE promoter-driven gene expression were further investigated using real-time RT-PCR (Supplementary Fig. S1, available in JGV Online). PD098059 treatment starkly reduced IFN-α-induced expression of 2′-5′-OAS in vector control and PLpro-expressing cells (Supplementary Fig. S1). Results confirmed a link between ERK1 activation and STAT1 signalling as the antagonism of IFN-α-induced ISRE-mediated gene expression by PLpro.

DISCUSSION

SARS-CoV does not induce type I IFN in cell culture, which may be crucial to pathogenesis of this virus. This study focused on one SARS-CoV protein, PLpro protease, earlier reported to have antagonistic activity in innate immune responses including synthesis of IFNs and cytokines (Devaraj *et al.*, 2007; Frieman *et al.*, 2009). We first demonstrated stable SARS-CoV PLpro expression in human promonocyte cells as well as inhibition of IFN-α-induced ISRE- and AP-1-driven promoter activity and reduction of IFN-stimulated gene expression (Figs 2 and 3). Results concurred with previous findings: SARS-CoV PLpro protein inhibited activity of IFN-β, ISRE and NF-κB promoters induced by poly I:C (Devaraj *et al.*, 2007; Frieman *et al.*, 2009). The antagonistic mechanism of SARS-CoV PLpro on these activities is controversial (Devaraj *et al.*, 2007; Frieman *et al.*, 2009). Devaraj *et al.* (2007) demonstrated PLpro interacting with IRF-3, blocking phosphorylation and nuclear translocation of IRF-3 and disrupting activation of type I IFN responses. Frieman *et al.* (2009) found PLpro not directly binding with IRF-3 or inhibiting *in vitro* phosphorylation of IRF-3.

This study used the proteomic approach to detect changes in protein expression in PLpro-expressing cells in the presence or absence of IFN-α (Fig. 4). PLpro expression in human promonocyte cells stimulated mRNA expression of UBC E2-25K (Fig. 5b), which could support the increase of protein level of UBC E2-25K in 2D gels (Fig. 4). PLpro expression caused 50 % decrease of ERK1, but not ERK2, in PLpro-expressing cells compared with vector controls (Fig. 6a), being associated with ubiquitin-dependent proteosomal degradation of ERK1, as confirmed by poly-ubiquitination of ERK1 and treatment with the proteosome inhibitor MG-132 (Fig. 6b, c). IFN-α treatment enhanced time-dependent manner of ERK1 downregulation, but the proteosome inhibitor MG-132 time-dependently restored IFN-α-enhanced degradation of ERK1 in PLpro-expressing cells, but not vector controls (Fig. 6a, c). With ERK1/2 signalling regulated by ubiquitin-proteasome system via degradation of ERK1/2 and the upstream MAP kinase kinase kinase 1 (MEKK1) by ubiquitination (Laine & Ronai, 2005; Lu *et al.*, 2002), those reports led us to identify ERK1 ubiquitination level in vector control and PLpro-expressing cells with or without IFN-α treatment (Fig. 6b). Interestingly, PLpro expression significantly increased ERK1 ubiquitination with poly-ubiquitin chains compared with vector control cells (Fig. 6b, lanes 1–2), while IFN-α treatment decreased ubiquitinated levels and protein amounts of ERK1 in PLpro-expressing cells, but not in vector control cells (Fig. 6b, lanes 3–4). Treatment with the proteasome inhibitor MG-132 restored protein amounts of ERK1 (Fig. 6c) and IFN-α-induced activation of ERK1-mediated signalling in PLpro-expressing cells (Fig. 8), in concordance with prior studies, i.e. ERK1/2 signalling regulated by ubiquitin-proteasome system via degradation of ERK1/2 and upstream MEKK1 by ubiquitination (Laine & Ronai, 2005; Lu *et al.*, 2002). Proteomic analysis identified downregulation of ERK1 that was ubiquitinated and degraded by upregulation of ubiquitin proteasome pathways in PLpro-expressing cells, being responsible for the mechanism of IFN-α antagonism by SARS-CoV PLpro.

The treatment with the proteasome inhibitor MG-132 reversed this inhibition of IFN-α-induced ERK1-mediated signalling by PLpro (Fig. 7), indicating a significant correlation between ERK1 and STAT1 in PLpro-expressing cells in response to IFN-α. Results concurred with prior studies, with phosphorylation at Ser727 of STAT1 by active ERK1 involved in IFN-α/β-induced response (Wang *et al.*, 2004a) and IFN-γ inflammatory response (Lombardi *et al.*, 2008; Matsumoto *et al.*, 2005). In addition, downregulation of ERK1 in PLpro-expression cells correlated with suppression of AP-1-driven luciferase activity, IL-6 and IL-8 mRNA expression and c-Jun phosphorylation in responses to IFN-β (Figs 3 and 7). Importantly, we confirmed the correlation of ERK1 and STAT1 signalling pathways by treatment of PD098059 (an ERK1/2 inhibitor) (Fig. 8). PD098059 treatment inhibited IFN-α-induced ERK1 and STAT1 phosphorylation in vector control and PLpro-expressing cells, as well as IFN-α-induced expression of 2′-5′-OAS in vector control and PLpro-expressing cells (Supplementary Fig. S1). In addition, the other ERK1/2 inhibitor U0126 was used to test the correlation between ERK1/2 and STAT1. ERK1/2 inhibitor U0126 significantly inhibited IFN-α-induced phosphorylation of STAT1 at Ser727 in vector control cells and PLpro-expressing cells (Supplementary Fig. S2, available in JGV Online). ERK1/2-mediated signalling proves elemental in EGF-induced survival response to antagonize IFN-α-induced apoptosis of cancer cells (Caraglia *et al.*, 2003). Downregulation of ERK1-mediated signalling by PLpro might thus be considered an escape mechanism of SARS-CoV against type I IFNs. Activation of ERK1-mediated signalling may improve innate immune response against SARS-CoV, being alternative targets for development of SARS therapy.

We also demonstrated the reduction of ERK1 protein level in human promonocyte cells 24 h post-infection with human coronavirus NL63 (HCoV-NL63) and reversion of ERK1 protein level in HCoV-NL63-infected cells after a 24 h incubation with IFN-α and the proteasome inhibitor MG-132 (Supplementary Fig. S3, available in JGV Online).

In addition, the reduction of IFN-α-induced phosphorylation of both ERK1 and STAT1 at Ser727 was confirmed in human lung adenocarcinoma epithelial A549 cells expressing SARS-CoV PLpro compared with vector control (Supplementary Fig. S4, available in JGV Online). Surprisingly, ERK2 that had consistently higher expression level than ERK1 in vector control and PLpro-expressing cells showed fewer amounts of protein level and IFN-α-induced phosphorylation in PLpro-expressing cells than vector control cells (Figs 6a, 7a and 8, Supplementary Fig. S4). The treatment with the proteasome inhibitor MG-132 reversed the amounts of ERK2 protein and the inhibition of IFN-α-induced ERK2 phosphorylation in PLpro-expressing cells (Figs 6c and 7b). Besides ERK1, ERK2 might be involved in type I IFN antagonism by SARS-CoV PLpro. ERK1 and ERK2 have approximately 85 % of amino acid identity co-expressed in virtually all tissues but with remarkably variable relative abundance, ERK2 as the predominant isoform in brain and haematopoietic cells (Milella *et al.*, 2003; Pagès & Pouysségur, 2004). Recent evidence suggests possible quantitative difference in ERK1 and ERK2 dynamics that could have a significant role in their regulation. Ectopic expression of ERK1, albeit not ERK2, attenuates Ras-dependent tumour formation in nude mice (Vantaggiato *et al.*, 2006). The properties of their cytoplasmic-nuclear trafficking showed ERK1 shuttles between nucleus and cytoplasm at a much slower rate than ERK2, correlating with reduced capability of ERK1 to carry proliferative signals to the nucleus (Marchi *et al.*, 2008). Constitutive activation of ERK2, but not ERK1, is critical for the acquired resistance to Imatinib Mesylate in chronic myelogenous leukaemia management (Aceves-Luquero *et al.*, 2009). In addition to cancers, Ebola virus envelope glycoprotein reduced phosphorylation and kinase activity of ERK2, but not ERK1, correlating with induction of cell death (Zampieri *et al.*, 2007). Vaccinia virus M2L protein blocks ERK2 phosphorylation, inhibiting virus-induced NF-κB activation (Gedey *et al.*, 2006). Type I IFN antagonism of SARS-CoV PLpro via ERK1 downregulation might thus be a unique mechanism useful in developing therapeutic agents against SARS-CoV infection.

In conclusion, stable SARS-CoV PLpro expression significantly suppressed IFN-α-induced responses. Upregulation of ubiquitin-proteasome pathway by SARS-CoV PLpro correlated with increase of ERK1 ubiquitination. IFN-α treatment elicited ERK1 degradation, then downregulated ERK1-mediated signalling in PLpro-expressing cells, resulting in negative regulation of STAT1 and AP-1 signalling pathways. Importantly, inhibition of ubiquitin proteasome function with MG-132 restored IFN-α-induced phosphorylation of ERK1, STAT1 and c-Jun, all suppressed by SARS-CoV PLpro. PD098059 treatment confirmed linkage between ERK1 activation and STAT1 signalling pathways as type I IFN antagonism by PLpro. Moreover, the study may provide novel insight into the molecular mechanism of IFN antagonism by SARS CoV PLpro.

METHODS

Cell culture and transfection. The SARS-CoV PLpro gene, located between nt 4507–5840 of the SARS-CoV TW1 strain genome (GenBank accession no. AY291451), was amplified by RT-PCR from genome RNA template, using primers 5′-CTCCGAATTCAACTC-TCTAAATGAGCCGCTTGTC-3′ and 5′-GAGGCTCGAGATCCTC-TGGGTCTTCAGGAGCGAGTTCTGGCTGTACGACACAGGCTTG-ATGGTTGTAGTG-3′. Forward primer contained an *Eco*RI restriction site, reverse primer included an *Xho*I restriction site and HSV epitope tag. Amplified RT-PCR product was cloned into pcDNA3.1/His C vector (Invitrogen), the resulting construct was named pSARS-CoV PLpro. The pSARS-CoV PLpro (4.5 μg) plus indicator vector pEGFP-N1 (0.5 μg) (Clontech) or pcDNA3.1 empty vector plus pEGFP-N1 were transfected into HL-CZ cells with GenePorter reagent. As per manufacturer's direction (Gene Therapy Systems), transfected cells were incubated for 5 h with a mixture of plasmid DNA and GenePorter reagent, then maintained in RPMI 1640 medium containing 20 % FBS. For the selection of the stably transfected cell line, cells were incubated with RPMI 1640 medium containing 10 % FBS and 800 μg G418 ml^{-1}. PLpro expression was detected by Western blotting of transfected cell lysates, using anti-HSV Tag mAb (Novagen) as a probe.

***In vitro trans*-cleavage activity of SARS-CoV PLpro.** The protease activity in SARS-CoV PLpro-transfected cells was determined by spectrophotometrically following digestion of substrate HRP containing the LXGG motif (Sigma). Transfected cell lysates (150 μl) were added to 150 μl of substrate reagent containing 0.01 μg ml^{-1} HRP in 50 mM Tris/HCl. After 1, 2, 3 and 4 h incubation at 37 °C, reaction mixtures were added to a 96-well plate and non-digested HRP activity was measured by adding chromogen solution containing 2,2′-azino-di-3-ethylbenzthiazoline-6-sulfonate and hydrogen peroxide. Relative *trans*-cleavage activity was calculated as $1-(A_{405\ \mathrm{PLpro}})/(A_{405\ \mathrm{no\ PLpro}})$.

Transient transfections of *cis*-reporter plasmids for signalling pathway assays. Plasmid pISRE-Luc *cis*-reporter was purchased from Stratagene. SARS-CoV PLpro-expressing and empty vector control cells were transfected with *cis*-reporter plasmid indicated, plus internal control reporter pRluc-C1 (BioSignal Packard) using the GenePorter reagent. After 4 h incubation with or without IFN-α2 (Hoffmann-La Roche), activity of experimental firefly luciferase and control *Renilla* luciferase was gauged by the Dual Luciferase Reporter Assay System (Promega) and TROPIX TR-717 Luminometer (Applied Biosystems) described by Lin *et al.* (2008).

2D gel electrophoresis and protein spot analysis. For 2D gel electrophoresis, empty vector control cells and PLpro-expressing cells incubated for 3 days in the presence or absence of 3000 U IFN-α ml^{-1} were harvested, washed twice with ice-cold PBS, and then extracted with lysis buffer containing 8 M urea, 4 % CHAPS, 2 % pH 3–10 non-linear (NL) IPG buffer (GE Healthcare), plus Complete, Mini, EDTA-free protease inhibitor mixture (Roche). After 3 h incubation at 4 °C, cell lysates were centrifuged for 15 min at 16 000 ***g***. Protein concentration of resulting supernatants was gauged with the Bio-Rad Protein Assay (Bio-Rad), 100 μg of protein sample diluted with 350 μl of rehydration buffer (8 M urea, 2 % CHAPS, 0.5 % IPG buffer pH 3–10 NL, 18 mM DTT, 0.002 % bromophenol blue), then applied to NL Immobiline DryStrips (17 cm, pH 3–10; GE Healthcare). First-dimensional isoelectric focus and second-dimensional electrophoresis were detailed in Lai *et al.* (2007), as was in-gel digestion to recover peptides from gel spots for nanoelectrospray mass spectrometry.

Nanoelectrospray mass spectrometry, data interpretation and database search. Proteins in spots of interest were identified using an Ultimate capillary LC system (LC Packings) coupled to a QSTARXL quadrupole-time of flight (Q-TOF) mass spectrometer

(Applied Biosystem/MDS Sciex). The nanoelectrospray mass spectrometry and database search were described previously (Lai *et al.*, 2007). Protein function and subcellular location were annotated by Swiss-Prot (http://us.expasy.org/sprot/) and proteins categorized according to their biological process and pathway, using the PANTHER Classification system (http://www.pantherdb.org) described in prior studies (Lai *et al.*, 2007; Varfolomeev *et al.*, 2007; Wang *et al.*, 2004a, b).

Western blotting and immunoprecipitation assays. To determine protein expression, lysates of PLpro-expressing cells and empty vector control cells incubated for 1 day in the presence or absence of 3000 U IFN-α ml^{-1} were mixed 1 : 1 with 2× SDS-PAGE sample buffer without 2-mercaptoethanol and boiled for 10 min. Proteins in the lysates were resolved by SDS-PAGE and transferred to nitrocellulose. Resulting blots were blocked with 5 % skimmed milk, then reacted with appropriately diluted antibodies, including rabbit anti-STAT1 (Cell Signalling), rabbit anti-phospho STAT1 (Ser727) (Abcam), rabbit anti-phospho STAT1 (Tyr701) (Abcam), anti-ERK1/2 mAb (Cell Signalling), anti-phospho-ERK1/2 mAb (Cell Signalling), rabbit anti-c-Jun (Abcam), rabbit anti-phospho c-Jun (Abacm) and anti-ubiquitin mAb (Zymed). Immune complexes were detected with HRP-conjugated goat anti-mouse or anti-rabbit IgG antibodies, followed by enhanced chemiluminescence detection (Amersham Pharmacia Biotech). To detect ubiquitination of ERK1, cell lysates were harvested and incubated with anti-ERK1 antibody for 4 h at 4 °C, followed by addition of protein A–Sepharose beads and additional 2 h of incubation. After collection by centrifugation, pellets were washed four times with NET buffer (150 mM NaCl, 0.1 mM EDTA, 30 mM Tris/HCl, pH 7.4); immunoprecipitated proteins were dissolved in 2× SDS-PAGE sample buffer without 2-mercaptoethanol and boiled for 10 min. Proteins were resolved by SDS-PAGE and transferred to nitrocellulose. Resulting blots were blocked with 5 % skimmed milk and then probed with rabbit anti-ERK1 (Zymed) and anti-ubiquitin mAb (Zymed) followed by enhanced chemiluminescence detection.

Quantification of IFN-β mRNA using real-time RT-PCR. Total RNA was isolated from PLpro-expressing cells and empty vector control cells incubated for 4 h in the presence or absence of 3000 U IFN-α ml^{-1}, using PureLink Micro-to-Midi Total RNA Purification System kit (Invitrogen). cDNA was synthesized from 1000 ng of total RNA, using oligonucleotide d(T) primer and SuperScript III reverse transcriptase kit (Invitrogen). To gauge expression in response to IFN-α, a two-step RT-PCR using SYBR Green I was used. Oligonucleotide primer pairs were (i) forward primer 5′-CAACCAGCGGTTGACTTTTT-3′ and reverse primer 5′-ATCCAGGAAGGCAAACTGAA-3′ for human PKR, (ii) forward primer 5′-GATGTGCTGCCTGCCTTT-3′ and reverse primer 5′-TTGGGGGTTAGGTTTATAGCTG-3′ for human 2′-5′-OAS, (iii) forward primer 5′-GATGGATGCTTCCAATCTGGAT-3′ and reverse primer 5′-AGTTCTCCATAGAGAACAACATA-3′ for human IL-6, (iv) forward primer 5′-CGATGTCAGTGCATAAAGACA-3′ and reverse primer 5′-TGAATTCTCAGCCCTCTTCAAAAA-3′ for human IL-8, (v) forward primer 5′-CTTCCCTGGCAAGCACTACC-3′ and reverse primer 5′-GTTTCGGGCTTCATGTTGA-3′ for human ERK1, and (vi) forward primer 5′-GCAATGACTCTCCGCACGG-3′ and reverse primer 5′-TCTGTTGCAGTCTCTACATCCC-3′ for human UBC E2-25K. In addition, glyceraldehyde-3-phosphate dehydrogenase (GAPDH) mRNA, a housekeeping gene, was measured using 5′-AGCCACATCGCTCAGACAC-3′ and 5′-GCCCCAATACGACCAAATCC-3′ as forward and reverse primers. Real-time PCR mixture contained 2.5 μl of cDNA (reverse transcription mixture), 200 nM of each primer in SYBR Green I master mix (LightCycler TaqMAn Master; Roche Diagnostics). PCR was performed with amplification protocol consisting of 1 cycle at 50 °C for 2 min, 1 cycle at 95 °C for 10 min, 45 cycles at 95 °C for 15 s, and 60 °C for 1 min. Amplification and detection of specific products were conducted in ABI Prism 7700 sequence detection system (PE Applied Biosystems). Relative changes in mRNA level of indicated genes were normalized relative to GAPDH mRNA.

Statistical analysis. Student's *t*-test or χ^2 test were used to analyse all data. Statistical significance between vector-control cells and PLpro-expressing cells was noted at $P<0.05$.

ACKNOWLEDGEMENTS

We would like to thank the National Science Council (Taiwan) and China Medical University for financial support (NSC96-2320-B-039-008-MY3 and CMU98-CT-22, CMU98-D-S-05, CMU98-P-03).

REFERENCES

Aceves-Luquero, C. I., Agarwal, A., Callejas-Valera, J. L., Arias-González, L., Esparís-Ogando, A., del Peso Ovalle, L., Bellón-Echeverria, I., de la Cruz-Morcillo, M. A., Galán Moya, E. M. & other authors (2009). ERK2, but not ERK1, mediates acquired and "de novo" resistance to imatinib mesylate: implication for CML therapy. *PLoS ONE* **4**, e6124.

Banninger, G. & Reich, N. C. (2004). STAT2 nuclear trafficking. *J Biol Chem* **279**, 39199–39206.

Barretto, N., Jukneliene, D., Ratia, K., Chen, Z., Mesecar, A. D. & Baker, S. C. (2005). The papain-like protease of severe acute respiratory syndrome coronavirus has deubiquitinating activity. *J Virol* **79**, 15189–15198.

Biron, C. A. (2001). Interferons alpha and beta as immune regulators–a new look. *Immunity* **14**, 661–664.

Caraglia, M., Tagliaferri, P., Marra, M., Giuberti, G., Budillon, A., Gennaro, E. D., Pepe, S., Vitale, G., Improta, S. & other authors (2003). EGF activates an inducible survival response via the RAS→Erk-1/2 pathway to counteract interferon-α-mediated apoptosis in epidermoid cancer cells. *Cell Death Differ* **10**, 218–229.

Deb, D. K., Sassano, A., Lekmine, F., Majchrzak, B., Verma, A., Kambhampati, S., Uddin, S., Rahman, A., Fish, E. N. & Platanias, L. C. (2003). Activation of protein kinase Cδ by IFN-γ. *J Immunol* **171**, 267–273.

Devaraj, S. G., Wang, N., Chen, Z., Chen, Z., Tseng, M., Barretto, N., Lin, R., Peters, C. J., Tseng, C. T. & other authors (2007). Regulation of IRF-3-dependent innate immunity by the papain-like protease domain of the severe acute respiratory syndrome coronavirus. *J Biol Chem* **282**, 32208–32221.

Frieman, M., Ratia, K., Johnston, R. E., Mesecar, A. D. & Baric, R. S. (2009). Severe acute respiratory syndrome coronavirus papain-like protease ubiquitin-like domain and catalytic domain regulate antagonism of IRF3 and NF-κB signaling. *J Virol* **83**, 6689–6705.

Gedey, R., Jin, X. L., Hinthong, O. & Shisler, J. L. (2006). Poxviral regulation of the host NF-κB response: the vaccinia virus M2L protein inhibits induction of NF-κB activation via an ERK2 pathway in virus-infected human embryonic kidney cells. *J Virol* **80**, 8676–8685.

Giannakopoulos, N. V., Luo, J. K., Papov, V., Zou, W., Lenschow, D. J., Jacobs, B. S., Borden, E. C., Li, J., Virgin, H. W. & Zhang, D. E. (2005). Proteomic identification of proteins conjugated to ISG15 in mouse and human cells. *Biochem Biophys Res Commun* **336**, 496–506.

He, L., Ding, Y., Zhang, Q., Che, X., He, Y., Shen, H., Wang, H., Li, Z., Zhao, L. & other authors (2006). Expression of elevated levels of pro-inflammatory cytokines in SARS-CoV-infected ACE2+ cells in SARS

patients: relation to the acute lung injury and pathogenesis of SARS. *J Pathol* **210**, 288–297.

Hoffmann, E., Dittrich-Breiholz, O., Holtmann, H. & Kracht, M. (2002). Multiple control of interleukin-8 gene expression. *J Leukoc Biol* **72**, 847–855.

Hsueh, P. R., Chen, P. J., Hsiao, C. H., Yeh, S. H., Cheng, W. C., Wang, J. L., Chiang, B. L., Chang, S. C., Chang, F. Y. & other authors (2004). Patient data, early SARS epidemic, Taiwan. *Emerg Infect Dis* **10**, 489–493.

Huang, K. J., Su, I. J., Theron, M., Wu, Y. C., Lai, S. K., Liu, C. C. & Lei, H. Y. (2005). An interferon-gamma-related cytokine storm in SARS patients. *J Med Virol* **75**, 185–194.

Lai, C. C., Jou, M. J., Huang, S. Y., Li, S. W., Wan, L., Tsai, F. J. & Lin, C. W. (2007). Proteomic analysis of up-regulated proteins in human promonocyte cells expressing severe acute respiratory syndrome coronavirus 3C-like protease. *Proteomics* **7**, 1446–1460.

Laine, A. & Ronai, Z. (2005). Ubiquitin chains in the ladder of MAPK signaling. *Sci STKE* **2005**, re5.

Lee, N., Hui, D., Wu, A., Chan, P., Cameron, P., Joynt, G. M., Ahuja, A., Yung, M. Y., Leung, C. B. & other authors (2003). A major outbreak of severe acute respiratory syndrome in Hong Kong. *N Engl J Med* **348**, 1986–1994.

Lin, C. W., Wu, C. F., Hsiao, N. W., Chang, C. Y., Li, S. W., Wan, L., Lin, Y. J. & Lin, W. Y. (2008). Aloe-emodin is an interferon-inducing agent with antiviral activity against Japanese encephalitis virus and enterovirus 71. *Int J Antimicrob Agents* **32**, 355–359.

Lindner, H. A., Fotouhi-Ardakani, N., Lytvyn, V., Lachance, P., Sulea, T. & Ménard, R. (2005). The papain-like protease from the severe acute respiratory syndrome coronavirus is a deubiquitinating enzyme. *J Virol* **79**, 15199–15208.

Lombardi, A., Cantini, G., Piscitelli, E., Gelmini, S., Francalanci, M., Mello, T., Ceni, E., Varano, G., Forti, G. & other authors (2008). A new mechanism involving ERK contributes to rosiglitazone inhibition of tumor necrosis factor-alpha and interferon-gamma inflammatory effects in human endothelial cells. *Arterioscler Thromb Vasc Biol* **28**, 718–724.

Lu, Z. & Hunter, T. (2009). Degradation of activated protein kinases by ubiquitination. *Annu Rev Biochem* **78**, 435–475.

Lu, Z., Xu, S., Joazeiro, C., Cobb, M. H. & Hunter, T. (2002). The PHD domain of MEKK1 acts as an E3 ubiquitin ligase and mediates ubiquitination and degradation of ERK1/2. *Mol Cell* **9**, 945–956.

Malakhov, M. P., Kim, K. I., Malakhova, O. A., Jacobs, B. S., Borden, E. C. & Zhang, D. E. (2003). High-throughput immunoblotting. Ubiquitiin-like protein ISG15 modifies key regulators of signal transduction. *J Biol Chem* **278**, 16608–16613.

Marchi, M., D'Antoni, A., Formentini, I., Parra, R., Brambilla, R., Ratto, G. M. & Costa, M. (2008). The N-terminal domain of ERK1 accounts for the functional differences with ERK2. *PLoS ONE* **3**, e3873.

Marra, M. A., Jones, S. J., Astell, C. R., Holt, R. A., Brooks-Wilson, A., Butterfield, Y. S., Khattra, J., Asano, J. K., Barber, S. A. & other authors (2003). The genome sequence of the SARS-associated coronavirus. *Science* **300**, 1399–1404.

Matsumoto, S., Hara, T., Hori, T., Mitsuyama, K., Nagaoka, M., Tomiyasu, N., Suzuki, A. & Sata, M. (2005). Probiotic Lactobacillus-induced improvement in murine chronic inflammatory bowel disease is associated with the down-regulation of pro-inflammatory cytokines in lamina propria mononuclear cells. *Clin Exp Immunol* **140**, 417–426.

Milella, M., Kornblau, S. M. & Andreeff, M. (2003). The mitogen-activated protein kinase signaling module as a therapeutic target in hematologic malignancies. *Rev Clin Exp Hematol* **7**, 160–190.

Nicholls, J. M., Poon, L. L., Lee, K. C., Ng, W. F., Lai, S. T., Leung, C. Y., Chu, C. M., Hui, P. K., Mak, K. L. & Lim, W. (2003). Lung pathology of fatal severe acute respiratory syndrome. *Lancet* **361**, 1773–1778.

Pagès, G. & Pouysségur, J. (2004). Study of MAPK signaling using knockout mice. *Methods Mol Biol* **250**, 155–166.

Ratia, K., Saikatendu, K. S., Santarsiero, B. D., Barretto, N., Baker, S. C., Stevens, R. C. & Mesecar, A. D. (2006). Severe acute respiratory syndrome coronavirus papain-like protease: structure of a viral deubiquitinating enzyme. *Proc Natl Acad Sci U S A* **103**, 5717–5722.

Rota, P. A., Oberste, M. S., Monroe, S. S., Nix, W. A., Campagnoli, R., Icenogle, J. P., Peñaranda, S., Bankamp, B., Maher, K. & other authors (2003). Characterization of a novel coronavirus associated with severe acute respiratory syndrome. *Science* **300**, 1394–1399.

Samuel, C. E. (2001). Antiviral actions of interferons. *Clin Microbiol Rev* **14**, 778–809.

Spiegel, M., Pichlmair, A., Martínez-Sobrido, L., Cros, J., García-Sastre, A., Haller, O. & Weber, F. (2005). Inhibition of beta interferon induction by severe acute respiratory syndrome coronavirus suggests a two-step model for activation of interferon regulatory factor 3. *J Virol* **79**, 2079–2086.

Sulea, T., Lindner, H. A., Purisima, E. O. & Ménard, R. (2005). Deubiquitination, a new function of the severe acute respiratory syndrome coronavirus papain-like protease? *J Virol* **79**, 4550–4551.

Tagliaferri, P., Caraglia, M., Budillon, A., Marra, M., Vitale, G., Viscomi, C., Masciari, S., Tassone, P., Abbruzzese, A. & Venuta, S. (2005). New pharmacokinetic and pharmacodynamic tools for interferon-alpha (IFN-alpha) treatment of human cancer. *Cancer Immunol Immunother* **54**, 1–10.

Tang, X., Gao, J. S., Guan, Y. J., McLane, K. E., Yuan, Z. L., Ramratnam, B. & Chin, Y. E. (2007). Acetylation-dependent signal transduction for type I interferon receptor. *Cell* **131**, 93–105.

Thiel, V., Ivanov, K. A., Putics, A., Hertzig, T., Schelle, B., Bayer, S., Weissbrich, B., Snijder, E. J., Rabenau, H. & other authors (2003). Mechanisms and enzymes involved in SARS coronavirus genome expression. *J Gen Virol* **84**, 2305–2315.

Tsang, K. W., Ho, P. L., Ooi, G. C., Yee, W. K., Wang, T., Chan-Yeung, M., Lam, W. K., Seto, W. H., Yam, L. Y. & other authors (2003). A cluster of cases of severe acute respiratory syndrome in Hong Kong. *N Engl J Med* **348**, 1977–1985.

Uddin, S., Sassano, A., Deb, D. K., Verma, A., Majchrzak, B., Rahman, A., Malik, A. B., Fish, E. N. & Platanias, L. C. (2002). Protein kinase C-δ (PKC-δ) is activated by type I interferons and mediates phosphorylation of Stat1 on serine 727. *J Biol Chem* **277**, 14408–14416.

Vantaggiato, C., Formentini, I., Bondanza, A., Bonini, C., Naldini, L. & Brambilla, R. (2006). ERK1 and ERK2 mitogen-activated protein kinases affect Ras-dependent cell signaling differentially. *J Biol* **5**, 14.

Varfolomeev, E., Blankenship, J. W., Wayson, S. M., Fedorova, A. V., Kayagaki, N., Garg, P., Zobel, K., Dynek, J. N., Elliott, L. O. & Wallweber, H. J. A. (2007). IAP antagonists induce autoubiquitination of c-IAPs, NF-κB activation, and TNFα-dependent apoptosis. *Cell* **131**, 669–681.

Wang, J. Y., Lee, C. H., Cheng, S. L., Chang, H. T., Hsu, Y. L., Wang, H. C. & Chu, S. H. (2004a). Comparison of the clinical manifestations of severe acute respiratory syndrome and Mycoplasma pneumoniae pneumonia. *J Formos Med Assoc* **103**, 894–899.

Wang, W. K., Chen, S. Y., Liu, I. J., Kao, C. L., Chen, H. L., Chiang, B. L., Wang, J. T., Sheng, W. H., Hsueh, P. R. & other authors (2004b). Temporal relationship of viral load, ribavirin, interleukin (IL)-6, IL-8, and clinical progression in patients with severe acute respiratory syndrome. *Clin Infect Dis* **39**, 1071–1075.

Wong, C. K., Lam, C. W., Wu, A. K., Ip, W. K., Lee, N. L., Chan, I. H., Lit, L. C., Hui, D. S., Chan, M. H. & other authors (2004). Plasma inflammatory cytokines and chemokines in severe acute respiratory syndrome. *Clin Exp Immunol* **136**, 95–103.

Yan, H., Xiao, G., Zhang, J., Hu, Y., Yuan, F., Cole, D. K., Zheng, C. & Gao, G. F. (2004). SARS coronavirus induces apoptosis in Vero E6 cells. *J Med Virol* **73**, 323–331.

Zampieri, C. A., Fortin, J. F., Nolan, G. P. & Nabel, G. J. (2007). The ERK mitogen-activated protein kinase pathway contributes to Ebola virus glycoprotein-induced cytotoxicity. *J Virol* **81**, 1230–1240.

Zhao, C., Denison, C., Huibregtse, J. M., Gygi, S. & Krug, R. M. (2005). Human ISG15 conjugation targets both IFN-induced and constitutively expressed proteins functioning in diverse cellular pathways. *Proc Natl Acad Sci U S A* **102**, 10200–10205.

Ziebuhr, J. (2004). Molecular biology of severe acute respiratory syndrome coronavirus. *Curr Opin Microbiol* **7**, 412–419.